(This is a sample cover image for this issue. The actual cover is not yet available at this time.)

Journal of Luminescence 131 (2011) 1885–1899

Contents lists available at ScienceDirect

Journal of Luminescence

journal homepage: www.elsevier.com/locate/jlumin

Separate and simultaneous binding effects of aspirin and amlodipine to human serum albumin based on fluorescence spectroscopic and molecular modeling characterizations: A mechanistic insight for determining usage drugs doses

Nooshin Abdollahpour [a], Ahmad Asoodeh [b], Mohammad Reza Saberi [c], JamshidKhan Chamani [a,*]

[a] Department of Biology, Faculty of Sciences, Mashhad Branch, Islamic Azad University, Mashhad, Iran
[b] Department of Chemistry, Faculty of Sciences, Ferdowsi University of Mashhad, Mashhad, Iran
[c] Department of Medical Chemistry, School of Pharmacy, Mashhad University of Medical Sciences, Mashhad, Iran

ARTICLE INFO

Article history:
Received 12 February 2011
Received in revised form
15 April 2011
Accepted 20 April 2011
Available online 30 April 2011

Keywords:
HSA
Aspirin
Amlodipine
Spectroscopy
Zeta potential
Molecular modeling

ABSTRACT

The binding of aspirin (ASA) and amlodipine (AML) to human serum albumin (HSA) in aqueous solution was investigated by multiple techniques such as fluorescence quenching, resonance light scattering (RLS), three-dimensional fluorescence spectroscopy, FT-IR and zeta-potential measurements in an aqueous solution at pH=7.4. For the protein–ligand association reaction, fluorescence measurements can give important clues as to the binding of ligands to proteins, e.g., the binding mechanism, binding mode, binding constants, binding sites, etc. Fluorescence spectroscopy showed that ASA and AML could quench the HSA fluorescence spectra, and this quenching effect became more significant when both ASA and AML coexisted. The results pointed at the interaction between HSA and both drugs as ternary systems decreasing the binding constant and binding stability of the HSA–drug complex as a binary system. Therefore, by reducing the amount of drugs transported to their targets, the free drug concentration of the target would be reduced, lowering the efficacy of the drugs. It was demonstrated that there exists antagonistic behavior between the two drugs when it comes to binding of HSA. Furthermore, the fluorescence results also showed that the quenching mechanism of HSA–drug complexes as binary and ternary systems is a static procedure. The number of binding sites of HSA–ASA, (HSA–AML)ASA, HSA–AML and (HSA–ASA) AML were 1.31, 0.92, 1 and 0.93, respectively. Due to the existence of the antagonistic action between ASA and AML, the binding distance *r* was reduced. The results of synchronous fluorescence and three-dimensional fluorescence spectra showed that the antagonistic action between ASA and AML would alter the micro-environment around Trp and Tyr residues. Moreover, the simultaneous presence of ASA and AML during binding to HSA should be taken into account in multidrug therapy, as it induces the necessity of a monitoring therapy owing to the possible increase of uncontrolled toxic effects. Molecular dynamic studies showed that the affinity of each of the drugs to HSA was reduced in the presence of significant amounts of the other. In the interaction of HSA with both drugs, the zeta potential of the ternary system is more negative than its binary counterpart. The zeta-potential results suggested induced conformational changes on HSA that confirmed the experimental and theoretical results.

1. Introduction

Protein binding plays an important role in the pharmacokinetics and pharmacodynamics of drug. The extent of protein binding in the plasma or tissue controls the volume of distribution and affects both hepatic and renal clearance. In many cases, the free drug concentration, rather than the total concentration in the plasma, is correlated to the effect. Drug displacement from drug–protein complexes can occur by direct competition of two drugs for the same binding site and is of importance for drugs that are highly bound (>95%), for which a small displacement of bound drugs can greatly increase the free drug concentration in the plasma [1]. Strong binding can decrease the concentration of free drugs in the plasma, whereas weak binding can lead to a low circulation time or poor distribution [2].

Albumin is one of the oldest known and probably most studied of all proteins. Its manifold diverse functions have attracted the interest of scientists and physicians for generations. Its applications are numerous, both in clinical medicine and in basic research [3,4]. HSA is the most abundant protein in blood plasma

* Corresponding author. Tel.: +98511 8437107; fax: +98511 8424020.
E-mail addresses: chamani@ibb.ut.ac.ir, chamaniJ@yahoo.com (J.K. Chamani).

0022-2313/$ - see front matter © 2011 Elsevier B.V. All rights reserved.
doi:10.1016/j.jlumin.2011.04.043

constituting about 60% of the total plasma protein. It plays a very important role in the binding of drugs in blood and it transports bound drugs to the tissue [5,6].

HSA plays a central part in the pharmacokinetics of drugs. Among the four aspects of pharmacokinetics (absorption, distribution, metabolism and excretion), distribution is controlled by this protein since most drugs that travel in plasma bind to HSA [7]. Therefore, knowledge of a drug's binding to albumin is very useful in therapeutic drug monitoring. The drugs bound to the protein possess prolonged times of action by preventing them from being metabolized; only un-bound drugs are pharmacologically active. The amount of drug molecules bound to the protein depends on the total drug concentration and its affinity to the protein. A few drugs bind to more than one site. There are also drugs that bind to anyone of the two sites. Since the binding of drugs to albumin is not selective, the simultaneous presence of two drugs can lead to competition. The drugs bind to the same site on HSA, and the un-bound fraction becomes higher due to competing interactions. The latter results in the displacement of one drug by another one from their high-affinity constant. At elevated concentrations, a drug can also bind to other sites and low-affinity sites can become active [5]. The sub-domain IIA of HSA (site I) possesses esterase activity, which can convert aspirin (acetyl salicylic) to salicylic acid. By means of nuclear magnetic resonance (NMR) spectroscopy, Honma reported that the hydrolysis rates of aspirin were greatly enhanced in the presence of HSA, thus confirming the esterase-like activity of HSA. The HSA residues involved were proposed to be Lys 199, but no further structural information is known [7].

The generic term of Aspirin® is acetyl salicylic acid (ASA), shown in Scheme 1. ASA also has an antiplatelet effect by inhibiting the production of thromboxane, which under normal circumstances binds platelet molecules together to repair damaged blood vessels. This is why ASA is used during prolonged periods, in low doses, to prevent heart attacks, strokes, and blood clot formation in people at high risk for developing blood clots [8]. It has also been established that low doses of aspirin may be given immediately after a heart attack to reduce the risk of another heart attack or of the death of cardiac tissue [9]. The main undesirable side effects of ASA are gastrointestinal ulcers, stomach bleeding, and tinnitus, especially when doses are high. In children and adolescents, ASA is no longer used to control flu-like symptoms or the symptoms of chickenpox or other viral illnesses, owing to the risk of Reye's syndrome [10]. Today, ASA is one of the most widely used medications in the world, with an estimated 40,000 metric tons consumed each year [11]. ASA has been theorized to reduce cataract formation in diabetic patients, but one study showed that it was ineffective for this purpose [12].

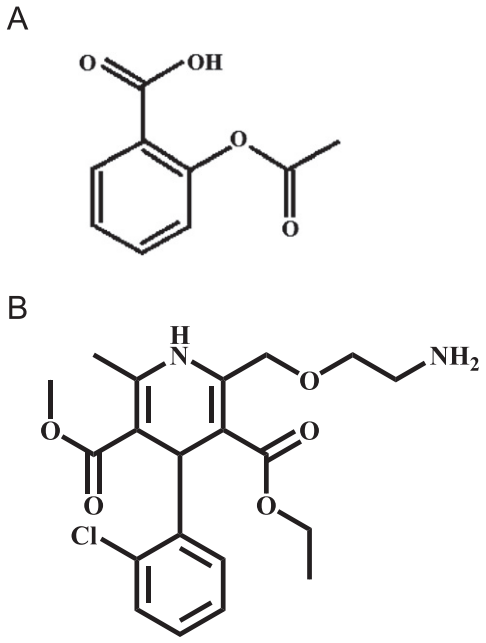

Scheme1. Chemical structures of (A) aspirin and (B) amlodipine.

Amlodipine (AML) besylate is the besylate salt of AML, a long-acting calcium channel blocker (Scheme 1B). AML is a dihydropyridine calcium antagonist (calcium ion antagonist or slow-channel blocker) that inhibits the trans-membrane influx of calcium ions into vascular smooth muscle and cardiac muscle. AML is a peripheral arterial vasodilator that acts directly on vascular smooth muscle to cause a reduction in peripheral vascular resistance and reduction in blood pressure [13]. The latter specifically interacts with membrane structures that ensure the release of Ca^{2+}, a well-known regulator of various physiological functions, such as vascular and bronchial tonus, myocardial contractility, atrioventricular conduction, etc. [14]. AML is widely utilized for the treatment of hypertension as well as stable and variant angina [15].

Binding of various drugs to HSA can result in a decrease or increase of their affinity. The aim of the present work was to determine the competition between ASA and AML at a specific high-affinity binding site with the use of the multi-technique. This analysis of the interaction between AML and ASA with HSA as binary and ternary systems constitutes the continuation of a study of HSA–drug binding in multidrug therapy.

2. Experimental section

2.1. Apparatuses

All fluorescence measurements were carried out on an F-2500 spectrophotometer (Hitachi, Japan) equipped with 1.0-cm quartz cells and a thermostat bath with a xenon lamp light. The excitation wavelengths were set to 280 and 295 nm. The excitation and emission slit widths were set to 5 nm. The scan speed was 1200 nm/min, and the PMT (Photo Multiplier Tube) voltage was 700 V. Fluorescence intensities were corrected for inner filter and dilution effects before analysis of the binding and quenching data. The RLS spectra was recorded with an F-2500 fluorescence spectrophotometer (Hitachi, Japan) by simultaneously scanning the excitation and emission spectra from 280 to 600 nm with $\Delta\lambda=0$ nm and a slit width of 5.0 nm, which has been proved to be able to investigate the aggregation of small molecules and the long-range assembly of drugs on biological templates. Synchronous fluorescence spectra were obtained by simultaneously scanning the excitation and emission monochromators. Such synchronous fluorescence spectra only show the Tyr and Trp residues of HSA when the wavelength interval ($\Delta\lambda$) is 15 and 60 nm, respectively. Three-dimensional fluorescence spectra were performed on an FP-2600 fluorescence spectrophotometer (Jasco, Japan) under emission and excitation wavelengths set between 220 and 500 nm with increments of 5 nm. The other scanning parameters were identical to those of the fluorescence quenching spectra. The UV/vis spectra were collected at room temperature on a double beam V-630 spectrophotometer (Jasco, Japan) in 1.0-cm quartz cells. The slit width was set to 5 nm, and the wavelength range was 200–500 nm.

Circular dichroism (CD) spectra were obtained on a J-815 Automatic Recording Spectropolarimeter (Jasco, Tokyo, Japan) with a quartz cell with a 2-mm path length at room temperature. The speed of scanning was 20 nm/min from 190 to 250 nm. Dry

nitrogen gas was used to purge the machine before and during the measurements. The bandwidth was 1 nm. The rotatory contributions of a protein can be determined by $X=f_HX_H+f_\beta X_\beta+f_RX_R$, where X can be either the ellipticity or the rotation at any wavelength, f is the fractions of the helix (f_H), beta form (f_β) and unordered form (f_R); the sum of f is equal to unity and each f is greater than or equal to zero. With the f values of five proteins obtained by X-ray diffraction studies, the X of the protein at any wavelength is filled by least-squares method, which defines the X_H, X_β, X_R. The CD for the helix, beta and random forms determined thus can be conversely used to estimate the secondary structure of any protein with X at several wavelengths for the same equation. The α-helical content (f_H) was estimated from the ellipticity value at 222 nm ($[\theta]_{222}$) as described as follows: $f_H=-([\theta]_{222}+2340/30300)$. The samples for CD were prepared with a fixed concentration of HSA (0.03%) and a varied drug concentration while maintaining equal volumes. The instrument was calibrated with ammonium d-10-camphor sulfunic acid. The induced ellipticity was obtained as the ellipticity of the HSA–drug mixtures after subtraction of the ellipticity of the drug at the same wavelength. It is expressed in degrees. The results are given as the mean residue ellipticity $[\theta]$, defined as $[\theta]=100\times\theta_{obsd}/(LC)$, where θ_{obsd} is the observed ellipticity in degrees, C is the concentration in residue Mol cm^{-3} and L is the length of the light path in the cell. All pH measurements were made with a Metrohm digital pH-meter (Metrohm, Germany). Infrared spectra were taken with a Bruker–Tensor 27 and infrared spectrometer equipped with a KBr beam splitter detector. The infrared spectrum was plotted against the inverse of the wavelength. The wavenumber, ν, which was proportional to the transition energy, had the unit cm^{-1}. The zeta-potential measurements were performed by using a Zeta-sizer, Nano-series–ZS (Malvern Instruments Ltd., UK). The primary source of experimentally determined protein structures was the Brookhaven Protein Data Bank [16] (the PDB code 1AO6) [17]. All the docking calculations were performed with the AutoDock 4.0 program on a Slax Linux workstation, while the Autodock tool (ADT) [18] was employed to prepare essential output files such as gpf, dpf and pdbqts. The structure of the ligands (ASA and AML) was built by Chem3D and the energy was minimized by HyperChem 7® [19].

2.2. Reagents

HSA (fatty acid free, 90%), ASA and AML were purchased from Sigma Chemical Co. (St. Louis, Mo. USA). All reagents were used as supplied without further purification. The protein was dissolved in 50 mM phosphate buffer at pH 7.4 and the stock solution was kept in the dark at 4 °C. All starting materials were of analytical reagent grade and double distilled water was used for all the measurements.

2.3. Procedures

ASA and AML were dissolved in the buffer and diluted to 0.05 and 0.002 mM, corresponding to low usage dose concentrations, respectively, with the solution consisting of 50 mM potassium phosphate pH 7.4. In measurements for each data point, 10 μl of the drug solution was added to 2 ml of the HSA solution (4.25×10^{-6} mM). The reaction time was investigated and the results showed that 3 min was enough for the stabilization. The fluorescence spectra were then measured (the excitation wavelengths were 280 and 295 nm and the emission wavelengths were 290–600 nm). The zeta-potential measurement and UV absorbance spectra of AML and ASA were recorded and spectral scanning curves were obtained under the same conditions.

3. Results and discussion

3.1. Fluorescence quenching of HSA by ASA and AML in binary and ternary systems

Fluorescence spectroscopy is a technique that is very sensitive (picogram quantities of a material can be detected) and well-suited for measurements in the real time domain. Fluorescence spectroscopy has found wide use in the study of physico-chemical properties of proteins, protein–ligand interactions and protein dynamics. This is because almost all proteins contain naturally fluorescent amino acid residues such as Tyr and Trp. Fluorescence spectroscopy is often the method of choice for studying properties such as stability, hydrodynamics, kinetics or ligand binding, because of its exquisite sensitivity [20]. It refers to any process that decreases the fluorescence intensity of a sample. Fluorescence quenching has been widely studied both as a fundamental phenomenon, and as a source of information for biochemical systems. These biochemical applications of quenching are due to the molecular interactions that result in quenching [21].

In proteins, the three aromatic amino acids Phe, Tyr and Trp are all fluorescent. A valuable feature of intrinsic protein fluorescence is the high sensitivity of Trp to its local environment. Changes in the emission spectra of Trp often occur in response to conformational transitions, subunit association, substrate binding or denaturation. These interactions can affect the local environment surrounding the indole ring. Trp can be quenched by externally added quenchers or by nearby groups within the proteins. Phe display the shortest absorption and emission wavelengths. Phe displays a structured emission with a maximum near 282 nm. Indole displays a substantial spectral shift upon forming a hydrogen bond to the imino nitrogen, which is a specific solvent effect. Additionally, indole can be quenched by several amino acid side chains. As a result, the emission of each Trp residue in a protein depends on the details of its surrounding environment.

Protein fluorescence is generally excited at the absorption maximum near 280 nm or at longer wavelengths. The absorption of proteins at 280 nm is due to both Tyr and Trp residues, whereas at wavelength longer that 295 nm, the absorption is primarily due to Trp. Trp fluorescence can thus be selectively excited at 295–305 nm. Tyr is often regarded as a rather simple fluorophore. However, under some circumstances, Tyr can also display complex spectral properties. Tyr emission is observable in some proteins, but it appears that excited-state ionization is not a major decay pathway for Tyr in proteins [21].

HSA also contains the second group of fluorophore Tyr residues. In order to determine if both Tyr and Trp residues were involved in the interaction with the drug, the fluorescence of HSA excited at 280 and 295 nm in the presence of the drug was compared. When an excitation wavelength of 280 nm was used, the fluorescence of HSA came from both Trp and Tyr residues whereas a 295 nm wavelength only excited the Trp residues [22].

The presence of ASA and AML causes the quenching of fluorescence of has and this can be seen in Fig. 1A and B. When a fixed concentration of HSA was titrated with varying amounts of quencher, a remarkable decrease of the fluorescence of HSA was observed; such a decrease in intensity is known as quenching and this quenching was concentration-dependent [23]. The maximum emission wavelengths of HSA were 340 and 342 nm, and these values decreased when increasing the ASA and AML concentrations from 0 nm to 1.8×10^{-4} and 8.5×10^{-3} mM, respectively.

The biochemical applications of fluorescence often utilize intrinsic protein fluorescence. Among biopolymers, proteins are unique in displaying useful intrinsic fluorescence. The observed fluorescence quenching of Trp and Try residues suggested that the HSA–ligand interaction changed the micro-environment of these

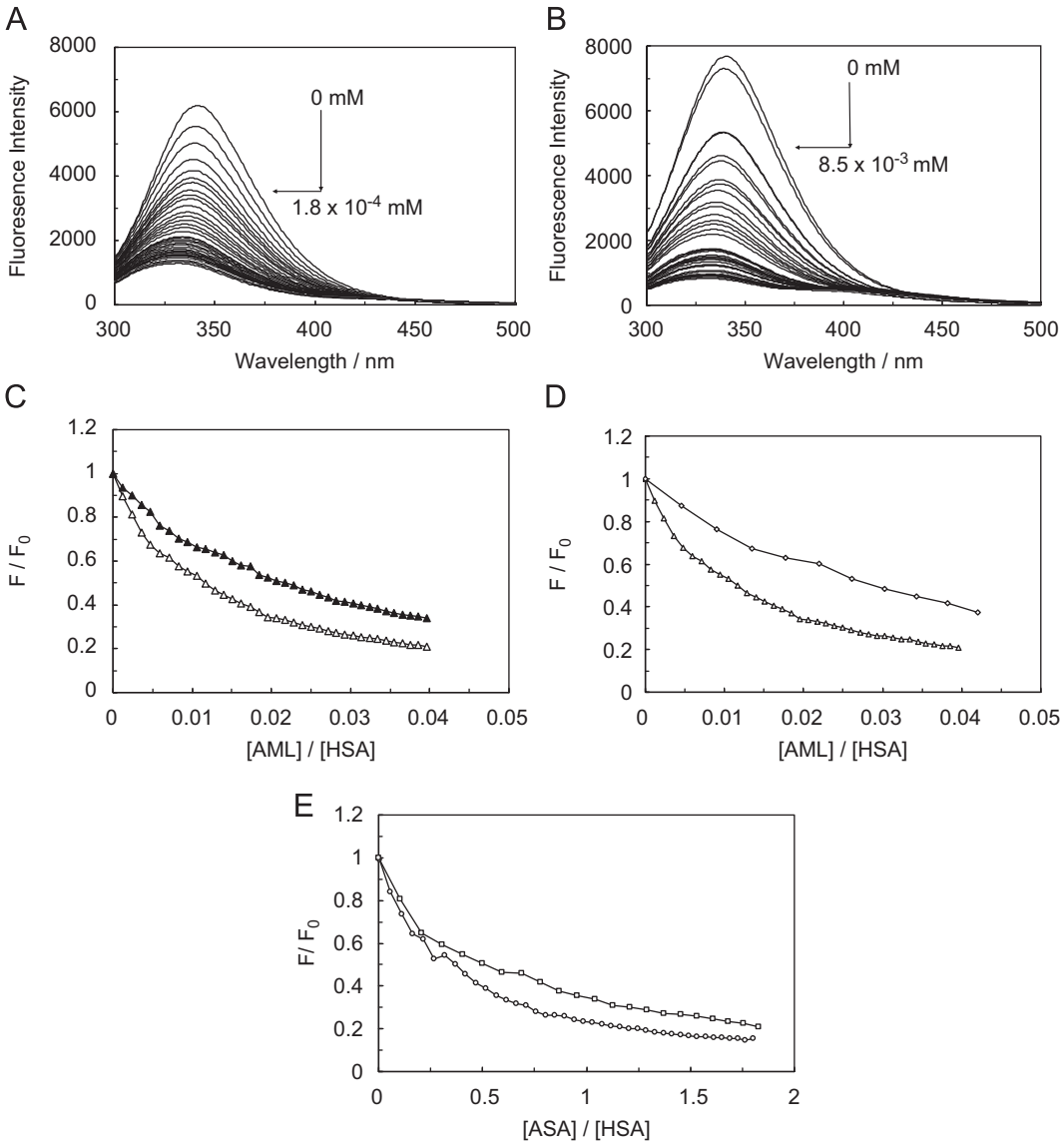

Fig. 1. Fluorescence spectra of (A) HSA–AML and (B) HSA–ASA complexes. Conditions: T=298 K, pH=7.4, λ_{ex}=280 nm, concentration of HSA was 4.5×10^{-3} mM and that of AML and ASA were increased from 1.8×10^{-4} mM and 0 to 8.5×10^{-3} mM, respectively (for the sake of clarity, the blue-shifts are shown with arrows). (C) a comparison of the quenching curves of HSA in the presence of various concentrations of AML obtained for excitation wavelength of 280 nm (Δ) and 295 nm (▲). (D) comparison of quenching curves of HSA in HSA–AML (Δ), (HSA–ASA)-AML (◇) systems at λ_{ex}=280 nm. (E) The comparison of quenching curves of HSA in HSA–ASA (○), (HSA–AML)-ASA (□) systems at λ_{ex}=280 nm. Conditions: T=298 K, pH=7.4, λ_{ex}=280 nm, c(HSA)=4.5×10^{-3} mM, c(AML)=0–1.8×10^{-4} mM, c(ASA)=0–8.5×10^{-3} mM.

residues. Moreover, the blue shift in the fluorescence spectra corresponded to a decreased polarity of the micro-environment after binding, which indicated that the chromophore of the protein was brought to more hydrophobic surroundings [24]. The quenching of HSA fluorescence by any ligand leads to the conclusion that this ligand can bind in the IIA sub-domain since in this albumin there is only one Trp, located in the IIA sub-domain. Additionally, by comparing the quenching curves obtained at excitation wavelengths of 280 and 295 nm for HSA–AML (Fig. 1C) complex, it can be clearly seen that they do not overlap and that the quenching curves of HSA excited at 280 nm were slightly higher than when excited at 295 nm. This phenomenon shows that in the interaction of ASA and AML with HSA, both the Trp and Tyr groups take part.

In order to determine the changes in the fluorescence of HSA bound with a drug in the presence of another drug, the quenching curves in the binary and ternary systems have been compared. Fig. 1D and E shows that the quenching curves of ternary systems, i.e., (HSA–ASA) AML and (HSA–AML)ASA, differ from the binary systems HSA–AML and HSA–ASA at both 280 and 295 nm. From Fig. 1D and E it can be concluded that when both Trp and Tyr are induced, the drug molecules approach Trp and Tyr in HSA. At an excitation wavelength of 280 nm, the fluorescence of HSA–AML was quenched more than in the ternary system and furthermore, Fig. 1E shows that the quenching curves did not overlap, indicating that both AML and ASA in the binary systems were located closer to Trp 214 than in the ternary systems. This means that only the Trp residue participated in both the HSA–ASA and (HSA–AML)ASA interactions, which may suggest that in the presence of another ligand, the structure of HSA changed, rendering the quantitative analysis impossible. The fluorescence quenching behavior could be analyzed using the Stern–Volmer equation of linear fittings [24]. Analysis of the modified Stern–Volmer equation (Eq. (1))

Table 1
Values of quenching constants, number of binding sites, fractional of accessible protein, R and r in the binary and ternary systems. Standard deviation value of K_Q was lower than usual values.

System	K_Q/M^{-1} λ=280 nm	K_Q/M^{-1} λ=295 nm	n λ=280 nm	n λ=295 nm	f_a λ=280 nm	f_a λ=295 nm	R	r/nm
HSA–ASA	1.03×10^6	4.15×10^5	1.31	0.98	1.19	0.90	0.997	1.87
(HSA–AML)ASA	$K_{QI}=3.36\times10^5$ $K_{QII}=6.14\times10^5$	3.82×10^3 9.60×10^3	0.92	0.87	1.06 0.86	1.01 0.62	0.994	1.83
HSA–AML	2.07×10^7	1.08×10^7	1.00	0.99	0.98	0.84	0.996	1.92
(HSA–ASA)AML	8.96×10^6	3.96×10^6	0.93	0.86	1.21	0.66	0.994	1.97

allowed us to determine the quenching constants K_Q and f_a for HSA–drug complexes [25].

The differing accessibilities of flourophore residues in proteins have resulted in the frequent use of quenching to resolve the accessible and inaccessible residues. Supposing that there are two populations of fluorophores, one of which is accessible (a) to quenchers and the other being inaccessible or buried (b) [21], the modified form of the Stern–Volmer equation allows f_a and K_Q to be determined graphically. The quenching constant K_Q is a quotient of an ordinate f_a^{-1} and slope $(f_a\ K_Q)^{-1}$ [26], and also a mean value of the quenching constants characterizing all binding sites of the HSA [25].

A plot of $F_0/\Delta F$ versus $1/[Q]$ yields f_a^{-1} as the intercept and $(f_a\ K_Q)^{-1}$ as the slope. A y-intercept of f_a^{-1} may be understood intuitively

$$F_0/\Delta F = 1/(f_a K_Q[Q]) + 1/f_a \quad (1)$$

In this case, ΔF is the difference in fluorescence in the absence and presence of the quencher at concentration $[Q]$, K_Q is the effective quenching constant for the accessible fluorophores [27], and f_a is the fraction of the initial fluorescence that is accessible to the quencher:

$$f_a = F_{0a}/(F_{0a}+F_{0b}) \quad (2)$$

In separation of the accessible and inaccessible fractions of the total fluorescence, it should be realized that there may be more than two classes of Trp residues. Also, even the presumed "inaccessible" fraction may be partially accessible to the quencher [21].

Table 1 shows that the f_a value was higher than when a 280-nm excitation wavelength was used. This suggests the participation of Tyr residues in the formation of a ligand–HSA complex [28]. For a limited range of quencher concentrations, the modified Stern–Volmer plot can still appear to be linear and provide a useful albeit arbitrary resolution of two assumed classes of Trp residues [21].

Based on the modified Stern–Volmer method, Fig. 2 presents a plot that is adjusted to estimate the quenching constants (K_Q) in complexes where the drug occupies more than one binding site. Sub-domains IIA and IIIA were the only binding site for ASA [29], and the quenching constant K_Q reflects the efficiency of quenching or the accessibility of the fluorophores to the quencher [21].

It was observed that ASA had two independent binding sites in HSA for an HSA–AML complex. Furthermore, as can be seen in Fig. 2B, the slope of the curves decreased with the addition of AML at a concentration corresponding to that in the HSA–ASA complex. This effect might suggest the weakening of the movement of molecules of both ligands in HSA [28]. The binding parameters, evaluated from the slope and intercept of these plots, are listed in Table 1. It can be seen that the number of binding site (n) was about 1 for all systems expect for the (HSA–AML)ASA complex, suggesting that one HSA molecule interacted with one ligand molecule. The comparison between K_Q values in binary and

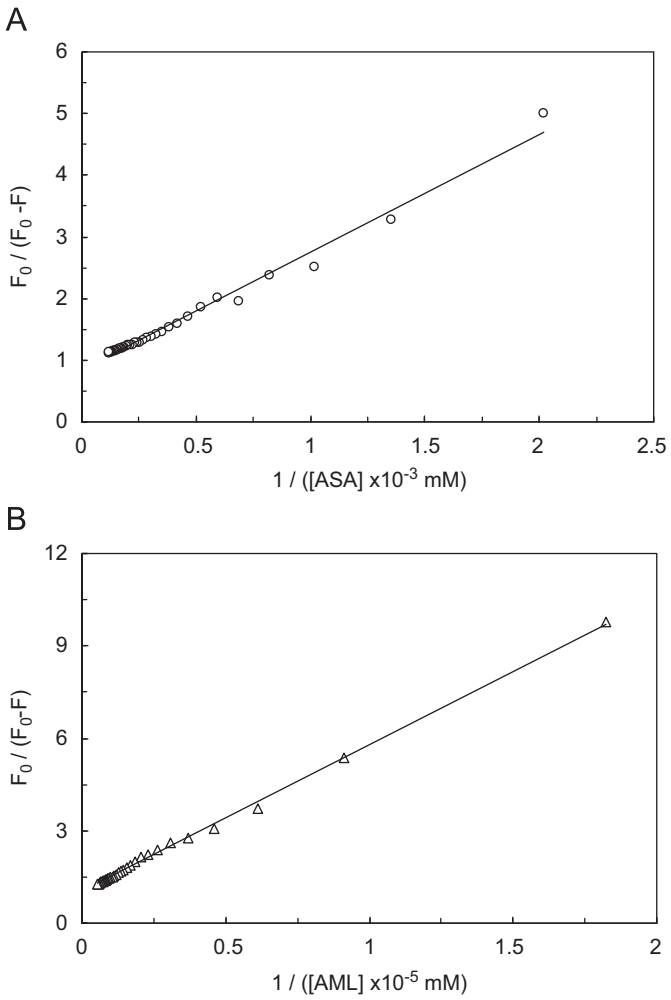

Fig. 2. Modified Stern–Volmer curves of fluorescence quenching of HSA, (A) HSA–ASA (○); (B) HSA–AML (Δ); systems. Conditions: T=298 K, pH=7.4, λ_{ex}=280 nm, c(HSA)=4.5×10^{-3} mM, c(AML)=0–1.8×10^{-4} mM, c(ASA)=0–8.5×10^{-3} mM.

ternary systems indicates that the K_Q value of HSA, during quenching by AML in binary and ternary systems, was greater than the corresponding value of another complex. This indicates that the binding of AML to HSA was quite strong and that the quenching process involved a static quenching mechanism [30].

The results of Table 1 point to the fact that, in the (HSA–AML)ASA complex, ASA has two types of binding sites in HSA. The comparison between K_Q in binary and ternary systems suggests that for the first type of binding site K_{QI}, K_{QII} decreased. It could thus be concluded that the interaction between ASA

and HSA in the ternary system was lower than in the binary system.

Based on the quenching constant values, it can be observed that interactions of HSA–ASA were very weak in comparison to the HSA–AML complex. Changes occurring in the HSA–AML complex influenced by the addition of ASA concentrations (Fig. 2A) differed from those observed in the (HSA–ASA)-AML complex (Fig. 2B). This effect might suggest a weakening of the movement of molecules within their binding sites, which was probably related to the presence of a large number of molecules of both ligands in sub-domains IIA and IIIA [28].

3.2. Synchronous fluorescence studies

The synchronous fluorescence spectroscopy technique was introduced by Lloyd in 1971 [31]. It involves the simultaneous scanning of the excitation and emission monochromators while maintaining a constant wavelength interval between them. Synchronous fluorescence spectroscopy gives information about the molecular environment in the vicinity of the chromospheres molecules and has several advantages, such as sensitivity, spectral simplification, spectral bandwidth reduction and the possibility of avoiding various perturbing effects. This is a useful method when studying the environment of amino acid residues by measuring the possible shift in wavelength emission maximum λ_{max}. Indeed, the shift in position of the emission maximum corresponds to changes of the polarity around the chromospheres molecule [32,33].

Synchronous fluorescence spectra are frequently used to characterize the interaction between small molecules and proteins since it can provide information about the molecular microenvironment in a vicinity of the chromospheres. When the D-value ($\Delta\lambda$) between excitation and emission wavelengths was stabilized at 15 or 60 nm, the synchronous fluorescence gives the characteristic information of Tyr or Trp residues [34]. According to Akusoba and Miller [35], the synchronous fluorescence of HSA is characteristic of a Trp residue with the $\Delta\lambda=60$ nm, and when $\Delta\lambda=15$ nm, the synchronous fluorescence of HSA is characteristic of a Tyr residue.

The effect of the drug on the synchronous fluorescence spectroscopy is shown in Fig. 3 It can be seen from Fig. 3A and B that the maximum emission wavelength has only a weak blue shift (about 1 nm) at the investigated concentration range when $\Delta\lambda=60$ nm. This could be an important hint to suggest conformational changes to has, which correspond to changes in polarity around the chromophore molecule during the formation of the ASA–HSA and AML–HSA complexes [36]. As for the Tyr residues (Fig. 3C and D), there was no shift of the maximum emission wavelength with $\Delta\lambda=15$ nm, which implies that the interaction of AML and ASA with HSA did not affect the conformation of the region around the Tyr residue [33]. On the other hand, the micro-environment around the Tyr residues has no discernable change during the binding process [35]. In consideration of the possible deviation introduced by the apparatus, no certain conclusions can be made regarding the changes of the micro-environment around the Tyr residues [35].

To explore the structural change of HSA induced by the addition of drugs, measurements were made of curves of F/F_0 versus [Q] (Fig. 3E–H) for the binary and ternary systems with various amounts of drugs (at $\Delta\lambda=60$ and $\Delta\lambda=15$ nm). Fig. 3E displays a higher slope of (HSA–ASA) AML, which indicated that the conformation of HSA and the polarity around the Trp residues had been altered. Furthermore, it was also shown in Fig. 3H that the slope of the (HSA–AML)ASA curve was higher when $\Delta\lambda$ was 15 nm, indicating a significant contribution of Tyr residues to the fluorescence of HSA. ASA was closer to the Tyr residues as compared to the Trp residues at the interface [33].

It can consequently be concluded that during the binding process of ASA with HSA in the presence of AML (ternary system), the drugs affected the micro-environment of the Trp residue but had no effect in the binary system. Moreover, in the (HSA–AML)ASA complex, the drugs influenced the micro-environment of the Tyr residues.

3.3. Resonance light-scattering spectra

In recent years, the resonance light-scattering (RLS) technique has gradually gained from the interest of analytical chemists. It is characterized by a high sensitivity, a convenience in performance and simplicity of the apparatus (usually a common spectrofluorometer). The RLS technique has been widely used on proteins [37]. In recent years, it was successfully applied to biochemistry, environment and food analysis and so on [38]. As a new spectral analysis technique, light-scattering measurements by using a common spectrofluorometer are very simple, and sensitive. The technique is generally coupled to other spectral analysis methods such as absorption, fluorescence and CD, and can compensate for the drawbacks of spectrophotometric and fluorometric measurements [39]. This attractive and promising approach has distinct advantages of speed, convenience and sensitivity. In recent years, more and more applications using RLS have been reported, including the study and determination of micro amounts of biomolecules, metal ions and drugs. Large numbers of correlative investigations have been completed and published before this work. For instance, investigations on nucleic acids, proteins, amino acids, saccharides, medicines, metal ions and even small bio-molecules like histidine all provided satisfactory results with the RLS technique. The RLS technique has already become a new analytical method characterized with high sensitivity, rapidity and simplicity [40]. This enhanced light-scattering signal can be measured using a common spectrofluorometer while simultaneously scanning the excitation and emission monochromators of a common spectrofluorometer with the wavelengths of the two monochromators being equal (namely $\Delta\lambda=0$) [39].

Fig. 4A shows that the RLS spectrum of HSA in the presence of AML demonstrates a sharp and maximum peak at 300 nm and two wide bands centering around on 340 and 370 nm. When AML was added to HSA, the RLS intensity was increased. It was observed that an interaction had occurred between HSA and AML and that it resulted in an increase of the RLS signal. The enhanced RLS intensity was proportional to the molecular weight of the proteins [39]. Fig. 4B and C displays the curves of ΔI_{RLS} versus the ligand concentration represented as $\Delta I_{RLS}=I_{RLS}-I^0_{RLS}$ (where I_{RLS} and I^0_{RLS} are the RLS intensities of the systems with and without ligands, respectively) [41]. The RLS intensity of the binary systems increased when raising the drug concentrations (see Fig. 4B and C) and decreased in the ternary systems. It may be concluded that an interaction occurred between HSA and the drugs in the binary and ternary systems and that larger particles were produced, which resulted in the enhancement of the RLS signals.

The addition of drugs in the binary systems also induced hydrophobic groups. The hydrophobic groups of the two-component complexes, i.e., HSA–ASA and HSA–AML, could interact with each other and aggregate together, which was the main reason for the enhanced RLS intensity of HSA [42]. In addition, as can be shown in Fig. 4B, when the AML concentration reached about 2.5×10^{-5} mM, AML aggregated on the HSA, and this value thus corresponded to the critical induced aggregation concentration (C_{CIAC}) of the drug [43].

As shown in Fig. 4B, the RLS intensity in the ternary system (HSA–ASA) AML gradually decreased with the increase in AML concentrations due to the reduction of the amount of negative charges on the surface of HSA. On the other hand, there was also

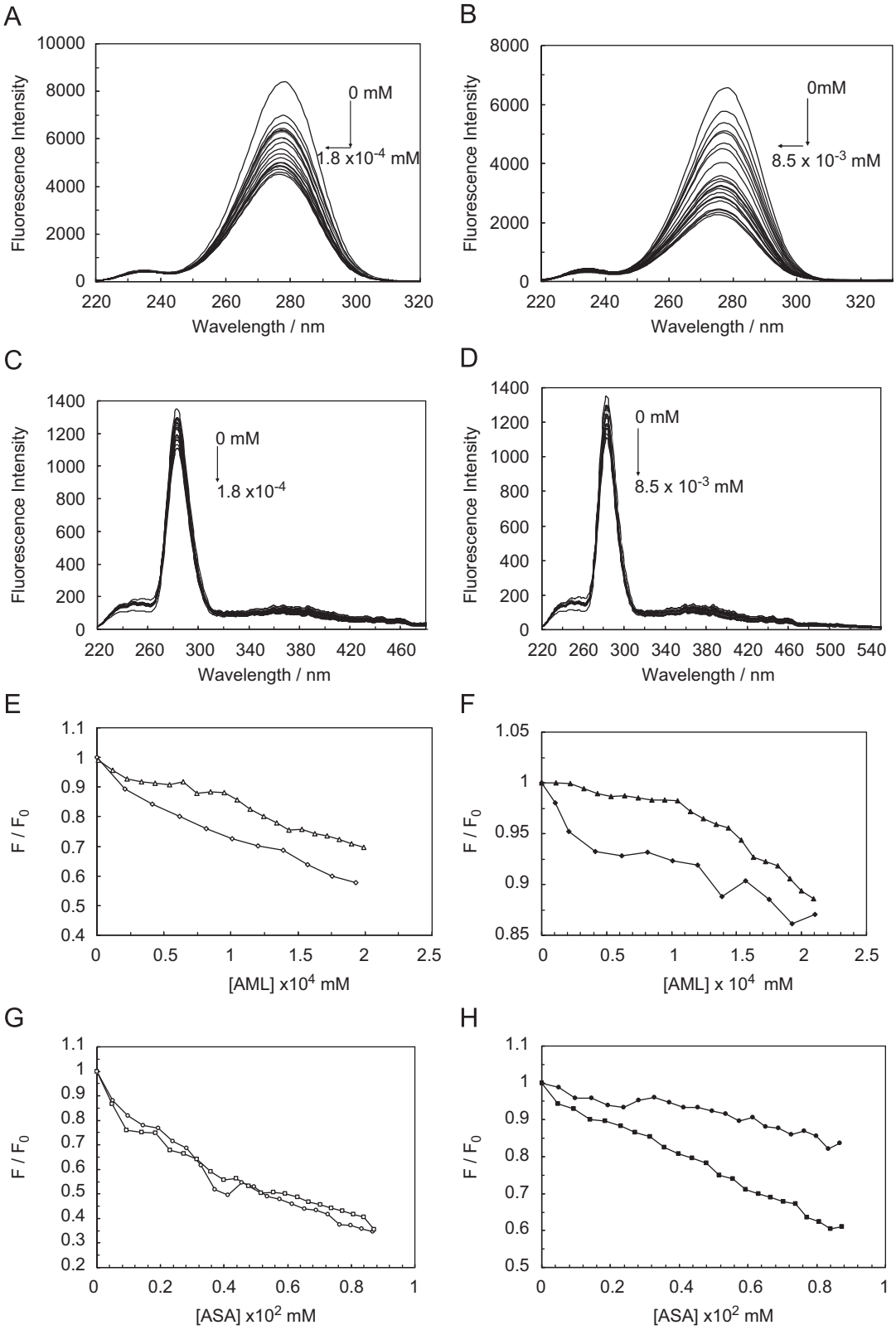

Fig. 3. Synchronous fluorescence spectra of HSA in the presence of (A) AML and (B) ASA, at $\Delta\lambda=60$ nm, and in the presence of (C) AML and (D), ASA at $\Delta\lambda=15$ nm under otherwise identical conditions; (E) comparison of curves of F/F_0 versus [Q] for the binary HSA–AML (Δ); ternary (HSA–ASA)-AML (◇) systems at $\Delta\lambda=60$ nm and (F) filled symbols correspond to $\Delta\lambda=15$ nm; (G) comparison of curves of F/F_0 versus [Q] for the binary HSA–ASA (○), ternary (HSA–AML)-ASA (□) systems at $\Delta\lambda=60$ nm and (H) filled symbols correspond to $\Delta\lambda=15$ nm.

a decrease of self-aggregation and an increase of the amount of dissolved protein in the presence of ASA as compared to for HSA–AML. Fig. 4C also shows that in the presence of AML in the ternary system (HSA–AML)ASA, the C_{CIAC} was higher than in HSA–ASA. This meant that AML caused a change in the behavior of interaction between HSA and ASA in the binary system.

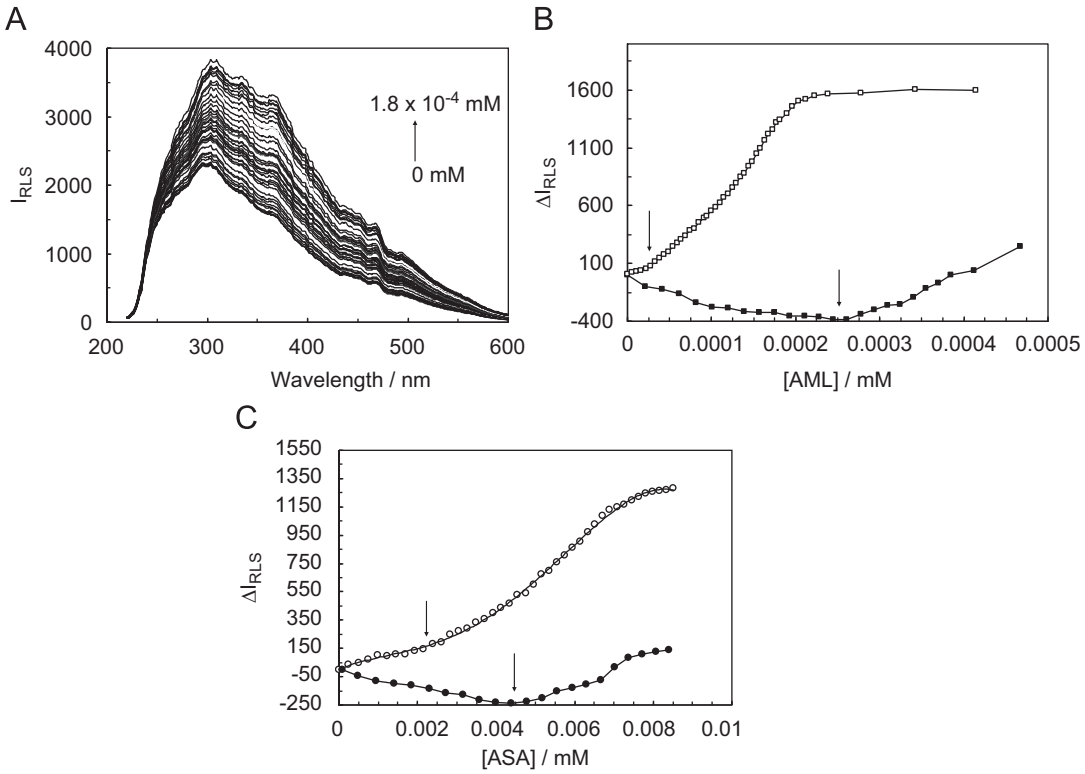

Fig. 4. (A) RLS spectra of HSA in the presence of increasing concentrations of AML from 0 to 1.8×10^{-4} mM**; (B) curves of ΔI_{RLS} versus [AML] for HSA–AML (□), (HSA–ASA)-AML (▲) systems; (C), The curves of ΔI_{RLS} versus [ASA] for HSA–ASA (○), (HSA–AML)-ASA (●) systems. Conditions: T=298 K, pH=7.4, c(HSA)=4.5×10^{-3} mM, c(AML)=0–1.8×10^{-4} mM, c(ASA)=0–8.5×10^{-3} mM.

3.4. Three-dimensional fluorescence spectra

Three-dimensional fluorescence spectroscopy is a new analytical technique that is applied to investigate the conformational changes of proteins. The excitation wavelength, the emission wavelength and the fluorescence intensity can be used as the axes rendering the investigation of the characteristic conformational changes of proteins more scientific and credible. The maximum fluorescence emission wavelength of amino acid residues in a protein is related to the polarity of the environment. Experiments have suggested that the fluorescence emission spectrum wavelength and the synchronous fluorescence spectrum wavelength of HSA in the absence and presence of drugs show distinct differences and sharp changes, which provide relative information on the configuration of the protein [44]. The three-dimensional spectra and contour maps of HSA and HSA–drug complexes as binary and ternary systems are presented in Fig. 5.

As can be seen in Fig. 5, peak *a* is the Rayleigh scattering peak ($\lambda_{ex}=\lambda_{em}$), and peak *b* is the second-order scattering peak ($\lambda_{ex}=2\lambda_{em}$). Peak 1 ($\lambda_{ex}$=280 nm, λ_{em}=345 nm) is the fluorescence peak and mainly enunciates the spectral behavior of Tyr and Trp residues, since excitation of HSA at 280 nm reveals the intrinsic fluorescence of Trp and Tyr residues, whereas the Phe residue fluorescence is negligible [45]. In comparison to peak 1, another fluorescence peak 2 (λ_{ex}=230 nm, λ_{em}=345 nm) has the characteristic polypeptide backbone structure of HSA [46]. When comparing the peaks for HSA in the two binary systems, we can see that the peak strength of peak 2 of HSA–AML and HSA–ASA is lower than the one in free HSA, which indicates that the polypeptide backbone structure of HSA has been changed in the presence of AML and ASA.

The strength of peak 1 and 2 in the ternary system was lower than in the free HSA. It indicates that the micro-environment has been altered during the formation of the complex in the presence of both drugs. Also, the intensity of peak *b* in the free HSA, as compared to the HSA–ASA complex, was decreased. In other words, the decrease in fluorescence intensity of the two peaks (peak *a* and *b*) in combination with the synchronous fluorescence spectra results, suggested that the slight unfolding of the peptides of protein induced a conformational change of the protein that increased the exposure of some hydrophobic regions which were previously buried [47]. Therefore, it was concluded that there occurred a specific interaction between HSA and both drugs in the binary and ternary systems.

3.5. Energy transfer from HSA to the drugs

Energy transfer can occur through direct electrodynamic interaction between a primary excited molecule and its neighbors. The spectroscopic method is suitable for measuring distances over several nanometers [48]. Photo-induced energy transfer between a donor and an acceptor can occur via Coulumbic interaction (Forster mechanism) and/or electronic exchange interaction (Dexter mechanism). Forster resonance energy transfer (FRET) has been extensively used in a number of fields, including biochemistry or medical diagnostic, since the favorable distances for FRET are comparable to the size of a protein or the thickness of a membrane. In medicinal chemistry, fluorescence emission has shown to be a very useful tool to gain insight into the interactions that take place between drugs and transport proteins. An interesting feature of proteins is that, in contrast to other bio-molecules, they display useful intrinsic fluorescence due to the presence of amino acids such as Phe, Tyr and/or Trp. In general, their fluorescence spectrum is dominated by Trp, which is highly sensitive to the local environment. Therefore, ligands binding to proteins can give rise to changes

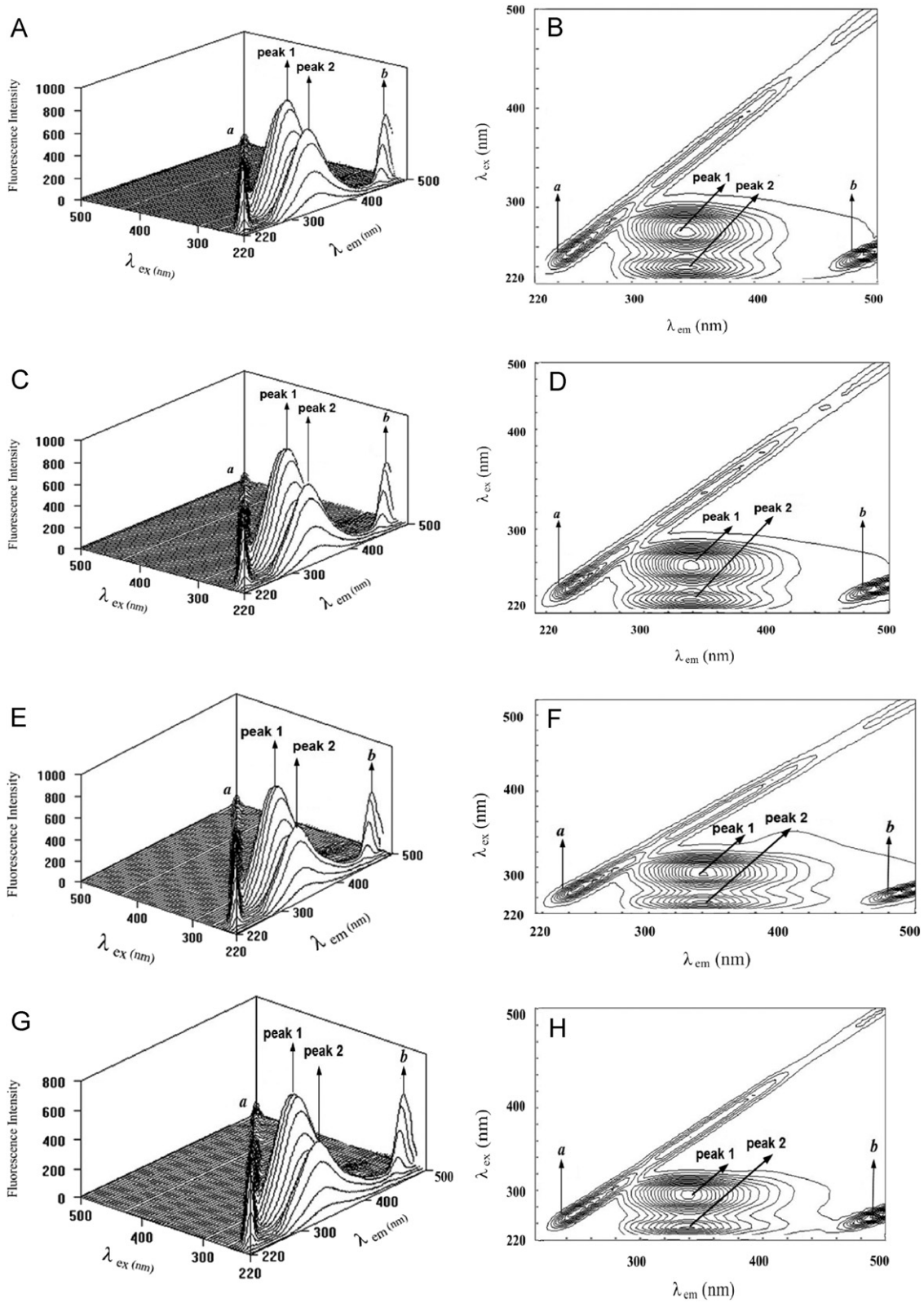

Fig. 5. Three-dimensional projections and the corresponding contour spectra of (A and B), free HSA; (C and D), HSA–AML; (E,F), HSA–ASA; (G and H), HSA–ASA–AML systems. Conditions: T=298 K, pH=7.4, c (HSA)=4.5×10^{-3} mM, c(AML)=0–1.8×10^{-4} mM, c(ASA)=0–8.5×10^{-3} mM.

of the Trp emission. In this context energy transfer can be used to determine the distance from a Trp residue to a complexed drug [49].

Using FRET, the binding distance r between the drug and the Trp residue of a protein can be calculated by the following equation:

$$E = 1-(F_0/F) = {R_0}^6/({R_0}^6+r^6) \quad (3)$$

Here, E is the efficiency of energy transfer between the donor and the acceptor, F and F_0 are the fluorescence intensities in the

presence and absence of the drug, respectively, and R_0 is the Forster critical distance when the efficiency of transfer is 50%, which can be calculated by the following equation:

$$R_0^6 = 8.8 \times 10^{-25} K^2 N^{-4} \Phi J \quad (4)$$

here, K^2 is the spatial factor of orientation of the transition dipoles, N is the refractive index of the medium and Φ is the fluorescence quantum yield of the donor [49]. It has been reported for HSA that, $K^2=2/3$, $E=0.18$, $\Phi=0.118$ and $N=1.336$ [50].

Fig. 6 shows an overlap between the absorption spectra of AML and ASA and the emission spectra of HSA. From Eq. (5), we can calculate the overlap integral J, which was 7.13×10^{-15} cm^3 mol^{-1} L for HSA.

$$J = (F(\lambda)\varepsilon(\lambda)\lambda^4 D\lambda)/(F(\lambda)D\lambda) \quad (5)$$

here, $F(\lambda)$ is the fluorescence intensity of the fluorescent donor at wavelength λ, $\Delta(\lambda)$ is the molar absorptivity of the acceptor at wavelength λ [51]. According to Eq. (4), the critical distances (R_0) were calculated as 3.2 nm for HSA. The parameters regarding the FRET are presented in Table 1. The energy transfer should most probably take place when the average distance between a donor fluorophore and an acceptor fluorophore is less than 10 nm [52], which means that $2<r<8$ nm [53] and $0.5\,R_0<r<1.5\,R_0$ [52]. Consequently, the distance between AML or ASA and Trp residue in HSA is 1.92 and 1.48 nm, respectively. Obviously, the distances are lower than 7 nm in interaction between HSA and AML or ASA [50].

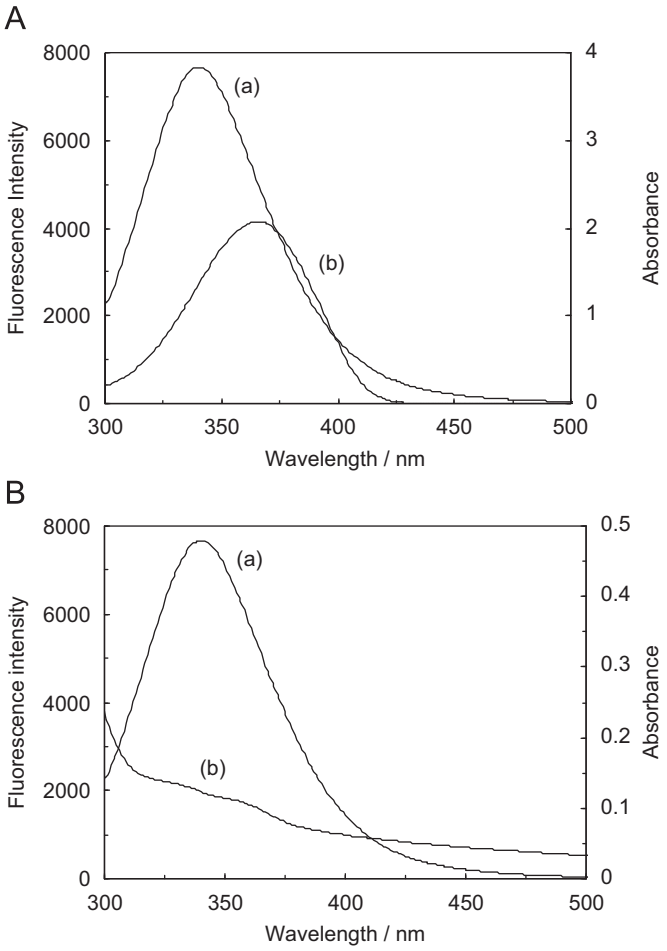

Fig. 6. Overlap of the fluorescence emission spectrum (curve a) of HSA with the absorption spectrum (curve b) for (A) HSA–AML and (B) HSA–ASA systems. c(HSA)=4.5 × 10^{-3} mM, c(AML)=1.8 × 10^{-4} mM, c(ASA)=8.5 × 10^{-3} mM.

This indicates that the energy transferred from HSA to the drugs occurs with a high probability [54].

Additionally, the distance between the drugs to HSA in the binary systems was shorter than in their ternary counterpart. In the presence of AML, the distance between ASA and HSA increased and in the presence of ASA, almost no effect occurred with regard to the distance between AML with HSA. In mechanisms and dynamics of fluorescence quenching, any process that causes a decrease in intensity can be considered to be quenching, and quenching results in the dissipation of the fluorophore's electronic energy as heat. Resonance energy transfer (RET) decreases the intensity of the donor and transfers the energy to an acceptor .The acceptor can be fluorescent or non-fluorescent, but in both cases, the fluorescence intensity of the initially excited molecule is decreased [21]. It can thus be concluded that it can be seen as the different conformational changes of HSA in the presence of the drugs in binary and ternary systems.

3.6. Circular dichroism and the conformational analysis

Circular dichroism (CD) is one of the most sensitive physical techniques for determining structures and for monitoring structural changes of bio-molecules. It can directly interpret the changes of a protein's secondary structure, even though the method is empirical. The far-ultraviolet (Far-UV) CD spectra (below 250 nm) of proteins are extremely sensitive toward protein structure, and the near-UV spectra reflect the contributions of aromatic side chains, disulfide bonds, and induced CD bands of prosthetic groups. Far-UV CD spectra have been used to show that the secondary structures of the molten globules resemble those of the corresponding native proteins [55].

There are four levels of protein structures [35]. The primary structure leads to the secondary structure; the local conformation of the polypeptide chain or the spatial relationship of amino acid residues that are close together in the primary sequence. In globular proteins, the three basic units of the secondary structure are the α helix, the β strand and turns [56]. Fig. 7 shows the changes in HSA α-helicity upon AML addition. The CD spectra of HSA exhibit two negative bands at 209 and 222 nm, which are characteristic of the α-helix [57]. The reasonable explanation is that the negative peaks at 209 and 222 nm are both contributed to by $n\rightarrow\pi$ transfer for the peptide band of the α-helix [58].

Table 2 lists the secondary structural elements that were calculated. Acquired data suggest that the secondary structure of free HSA consisted of ~53.84% α-helix, ~18.36% β-sheet, ~13.55% turn and ~14.25% unordered coil. The results in Table 2 show that the percentage of α-helix decreased gradually, from 53.84 in free HSA to 53.02% upon AML binding, indicating a certain degree of unfolding. Similar results were observed upon the binding of ASA and AML in binary and ternary systems to HSA, as shown in Table 2. From the above results, it was apparent that the binding of AML to HSA caused a conformational change of the protein, with the loss of α-helix stability. Furthermore, it can be concluded that the occupancy of the Trp sites by the binding ligands could actually stabilize the native conformation of the protein [59].

3.7. FT-IR spectra

Infrared spectroscopy has long been used as a powerful method for investigating the secondary structures of proteins and their dynamics [60]. The most significant advantage of FT-IR spectroscopy for biological studies is that spectra of almost any biological system can be obtained in a wide variety of environments, and that FT-IR is a technique for the study of hydrogen bonding [61]. In the IR region, i.e., the frequencies of bands due to the amide I–III vibrations [60],

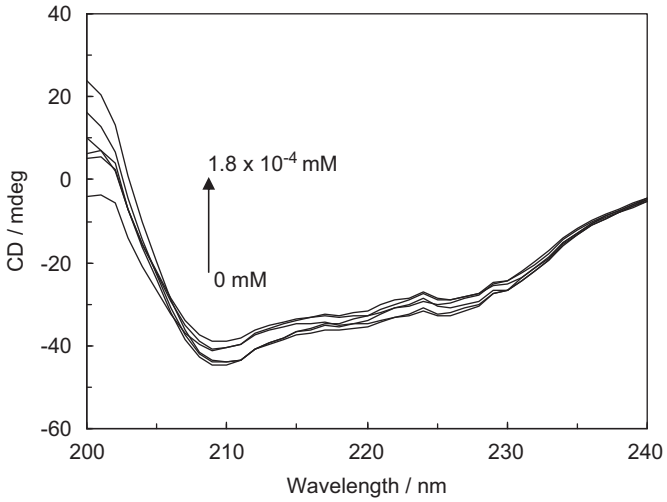

Fig. 7. Far-UV CD spectra of free HSA in the presence of various concentration of AML. Conditions: $T=298$ K, pH=7.4, c(HSA)=4.5×10^{-3} mM, c(AML)=0–1.8×10^{-4} mM.

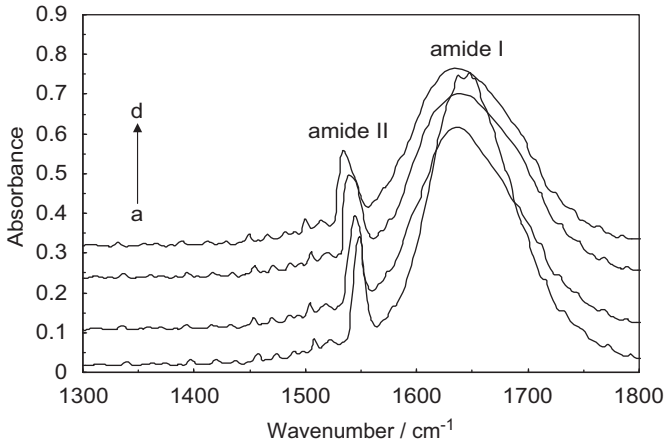

Fig. 8. Infrared (FT-IR) spectrograms of HSA in the presence of drugs in aqueous solution. (a) FT-IR spectrum of free HSA; (b) HSA–ASA; (c) HSA–AML; (d) HSA–AML-ASA systems. Conditions: $T=298$ K, pH=7.4, c(HSA)=4.5×10^{-3} mM, c(AML)=0–1.8×10^{-4} mM, c(ASA)=0–8.5×10^{-3} mM.

Table 2
Secondary structural analysis of the binary and ternary systems from CD data.

System	α-helix %	β-sheet %	Turn %	Unordered coil %
HSA	53.84	18.36	13.55	14.25
HSA–AML	53.02	18.22	13.38	15.38
HSA–ASA	51.38	18.07	13.49	17.06
(HSA–ASA)AML	48.57	18.14	13.04	20.25
(HSA–AML)ASA	46.53	17.09	12.95	23.43

the amid I bands is more sensitive to changes in the protein secondary structure than its amid II counterparts. Changes in the structure of the protein are reflected by changes in the component band positions of the amid I region [62]. The protein amide I band at 1650–1654 cm^{-1} (mainly due to C=O stretching) and the amide II band at 1560–1570 cm^{-1} (C–N stretch coupled with N–H bending mode) also bore a relationship with the secondary structure of proteins. In general, the spectral range from 1650 to1662 cm^{-1} in amide I bands can be attributed to α-helices [63].

In this work, the FT-IR spectrum of free HSA was acquired by subtracting the absorption of the phosphate buffer from the spectrum of the protein solution, which exhibited the characteristic amide I and amide II absorption bands at 1647 ± 0.5 and 1555 ± 0.5 cm^{-1}, respectively, as shown in Fig. 8. It was clear that, when adding ASA and AML to the binary system, the amide I and II bands shifted from 1647 to 1652 cm^{-1} and 1555 ± 0.5 to 1566 ± 0.5 cm^{-1}, respectively. In addition, a new peak appeared at 1531 ± 0.5 cm^{-1}, indicating that the change of the secondary structure of HSA was attributed to the addition of the drugs [64]. The peak positions of amides I and II were shifted upon the addition of ASA to the protein. For the HSA–ASA system in the presence of AML, the amid I band was shifted from 1660 ± 0.5 to 1643 ± 0.6 cm^{-1} while the amide II peak was shifted from 1540 ± 0.7 to 1530 ± 0.9 cm^{-1}.

These shifts indicate that the α-helical region of HSA was perturbed due to the interaction of ASA with HSA. These results pointed at ASA interacting with both the CO and CN groups in the protein polypeptides. The (HSA–AML)ASA complexes caused the rearrangement of the polypeptide carbonyl hydrogen-bonding network and finally led to the reduction of the protein helical structure. The content of β-sheet and turn of HSA decreased, while the content of the structural composition of HSA indicating α-helix, random coil, etc, increased when the molar concentration ratio of HSA to drug was enhanced [62].

3.8. Zeta-potential measurement

The zeta potential is widely used for quantifying the magnitude of the electrical charge at the double layer. The zeta potential, unlike the particle size or molecular weight, is a property involving not only the particles but also their environments, e.g., pH, ionic strength, and even the type of ions in the suspension [65]. The zeta potential is measured by electrophoresis or alternatively by streaming potential methods [66]. Such measurements have been used to obtain a correlation against aggregation results [67]. The result of a zeta-potential measurement is the potential of a material in an ionic solution at the boundary between the Stern layer and the diffuse layer. Larger positive values of the zeta potential at a fixed pH indicate a positive charge of the surface which would attract negatively charged entities such as anions or charged proteins while lower values of the zeta potential at a fixed pH reflect a negative charge of a material surface that tends to attract positively charged particles [68].

The zeta potential was calculated from the electrophoretic mobilities, μ_E, using the Henry equation:

$$Z=3\,\mu E\eta/2\varepsilon_0\varepsilon_r\times1/f(ka) \quad (7)$$

where ε_0 is the permittivity of vacuum, ε_r and η are the relative permittivity and viscosity of water, respectively, a is the particle radii and k is the Debye length. The function $f(ka)$ depends on the particle shape and for our systems, it was determined by:

$$f(ka)=2/3\text{-}9/2ka+75/2k^2a^2-330/k^3a^3 \quad (8)$$

and was valid for $ka>1$ [69]. To our knowledge, there are not yet any reports on the zeta potential of ASA and AML with HSA. These results are illustrated in Fig. 9, which shows a plot of the zeta potential of the protein–drug complexes as a function of the drug concentration. From Fig. 9A and B, it can be seen that there occurs interactions of HSA with ASA and AML in the binary (open symbols) and ternary (filled symbols) systems, and this is also proved by the zeta potential of these systems at different concentrations of AML and ASA. The zeta-potential values of HSA upon interaction with AML and ASA in the binary systems increased with raised concentrations of the drugs and then decreased continuously. On the other hand, the zeta-potential

values in the ternary systems acted differently. It was suggested that the AML or ASA molecules were bound with the association complex by hydrophobic forces. However, increasing amounts of drugs reduced the number of amino groups on the surface of HSA and also decreased the zeta potential of the system, consequently causing the contribution of the negatively charged carboxylic groups to become stronger and the zeta potential to be lowered [70].

On the other hand, when the drug concentration increased, the initial protein negative charge was reduced, which suggested the formation of protein–drug complexes. This trend was also indicative of the existence of electrostatic interactions between the protein and the drug molecules [2]. On the contrary, in the ternary systems, increasing amounts of a second drug at first reduced the number of amino groups on the surface of HSA and also decreased the zeta potential of the carrier system. Subsequently, the zeta potential slightly increased due to adsorption of the positively charged drug. This increase in repulsive forces might also result in an increase in the intermolecular forces that produced aggregation of the protein–drug complexes, as seen by RLS [71]. It was also observed that the formation of the large (HSA–ASA) AML complex could give rise to the great enhancement of RLS, indicating that electro-neutralization occurred, thus increasing the positive zeta potential, which corresponded to the formation of a large aggregate.

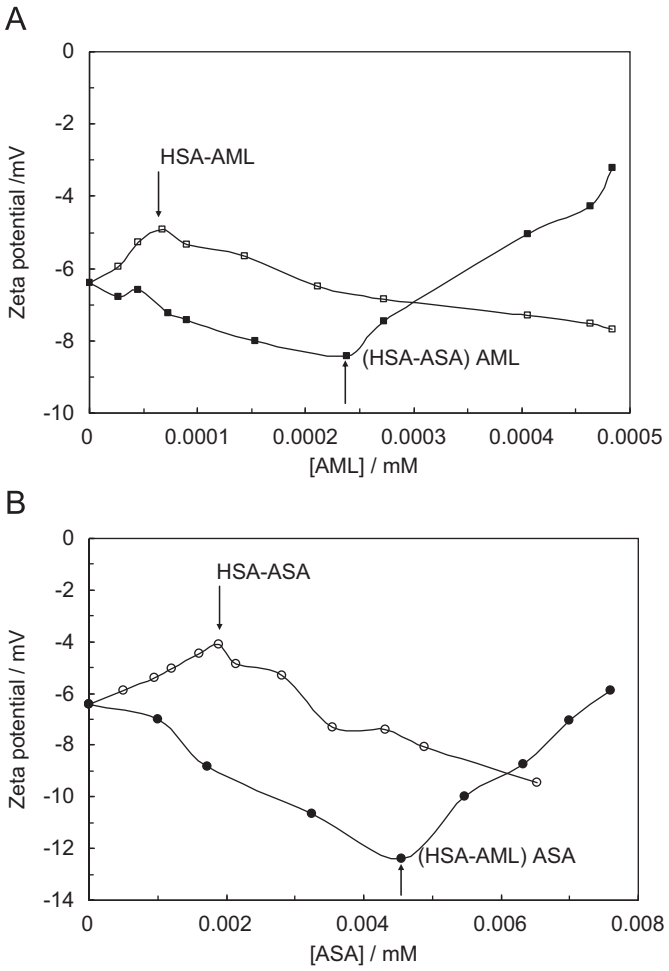

Fig. 9. Dependence of the zeta potential of HSA on the drug concentration. (A) HSA–AML (○); (HSA–ASA)-AML (●) and (B) HSA–ASA (□); (HSA–AML)-ASA (▲) systems. Condition: T=298 K, pH=7.4, c (HSA)=4.5×10^{-3} mM, c(AML)=0–1.8×10^{-4} mM, c(ASA)=0–8.5×10^{-3} mM.

3.9. Molecular modeling

Recent studies have shown that HSA is able to bind multiple ligands in several binding sites [72]. Six binding sites for various ligands were found in the HSA structure and drugs usually bind with high affinity to sites I and II [4]. The degree of displacement of drugs is dependent on their binding affinity constant. At elevated concentrations, a drug can also bind to other sites rendering low-affinity sites active.

Molecular modeling was carried out to complement the experimental data. In this work, only polar hydrogens were added to the protein. Moreover, Kollman united-atom partial charges were assigned and all water molecules were removed from the protein file in AutoDock Tools. Partial atomic charges were then calculated using the Gasteiger–Marsili method [73]. The Lamarckian genetic algorithm (LGA) program was utilized to calculate the conformational possibilities between the ligands and HSA. The docking parameter files for all docking procedures were generated by adopting the Lamarckian genetic algorithm method while the number of GA runs was set to 100 for each set. The population size was set to 150. In order to determine the possible conformation interaction for HSA, the grid parameter file was generated for the whole protein. The grid map was calculated using Auto Grid and finally the best docking energy results were assumed as the possible candidates for ligand–protein interaction.

The best results in dock, based on the lowest level of energy, are shown in Table 3 ASA displayed less affinity to the protein than AML. Fig. 10 exhibits the results of the drugs' interaction with HSA. The results are ranked by energy, and as shown in the figures, there were large hydrophobic cavities in HSA of which one of the largest was in the sub-domain IIA where the drugs can bind. The drugs were accommodated into a pocket surrounded by hydrophobic residues (Trp214, Leu219, Phe223, Leu234, Leu238, Leu260, Ile264, Il290 and Ala291) [74]. According to the lowest number of K_i (inhibition constant), ASA was located in subdomain IIA close to Lys199, while AML was located in a different site, called site II, near Asp255 (data not shown).

In the next step, when binary systems for HSA–ASA and HSA–AML were generated, the ternary docking was performed after energy minimization of the binary systems using a molecular mechanics method in the Hyperchem software (Fig. 10A and B) according to evaluation scores, until the best structure was

Table 3
Best ranked results of the parameters for the interaction of HSA with ASA and AML in the binary and ternary systems at pH=7.4 by the Autodock procedure.

System	K_i	Binding energy (kcal/mol)	Intermolecular energy (kcal/mol)	Electrostatic energy (kcal/mol)	Hydrogen bonds with
HSA–ASA	651.74 μM	−4.35	−5.08	−1.22	Lys199
(HSA–AML)ASA	84.81 pM	−13.47	−14.32	−11.64	no
HSA–AML	18.64 μM	−6.45	−7.18	−4.02	Asp255 Asp259
(HSA–ASA)AML	52.71 mM	−1.74	−1.76	−2.24	Glu311

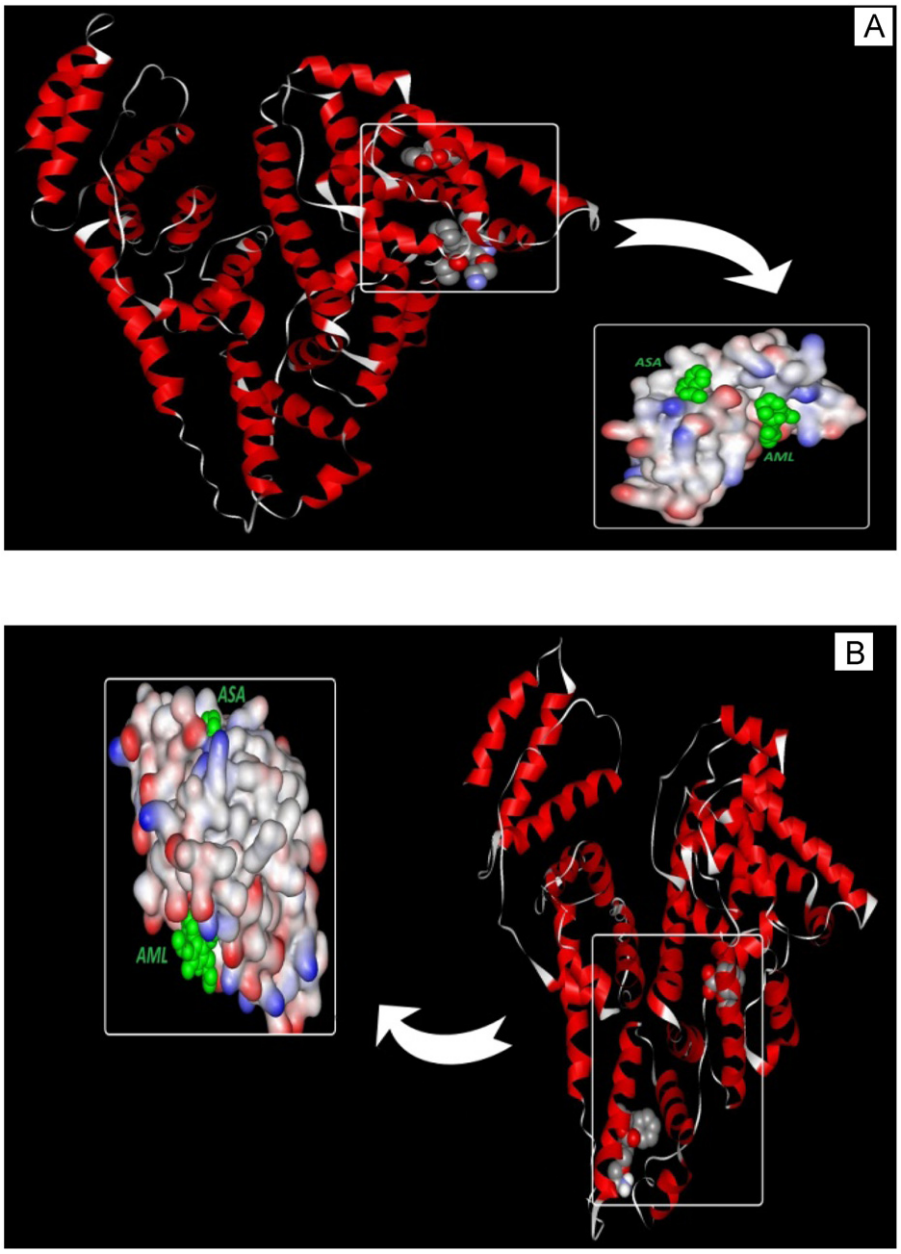

Fig. 10. Docking interaction of (A) HSA–ASA; (B) HSA–AML as binary systems; (C) (HSA–AML)ASA; (D) (HSA–ASA) AML as ternary systems. Drugs are shown as CPK and the surface of the protein is color-coded according to the hydrophobicity of the residue.

obtained. RMSD was taken into account in order to compare the natural HSA versus the minimized HSA. An RMSD of 0.4 Ångstrom defined little change in the minimized protein.

As shown in Table 3, the inhibitory constant was remarkably decreased after addition of ASA to the HSA–AML complex. Although each drug was located in a different position and they had a non competitive interaction, they affected each other's affinity. It was assumed that the fact that ASA and AML occupied different active sites changed the secondary structure of HSA. Our theoretical results were supported by experimental evidence such as far-UV CD. On the other hand, in the (HSA–ASA) AML system, each drug separately altered the conformation of the protein whereas in (HSA–AML)ASA, both drugs were involved in modifying the protein conformation. As observed from the CD results, ASA changed the helical structure of HSA more than AML did (nearly 2.5%). We assume that AML was unable to bind to HSA properly because of its large size, thus giving rise to a lower affinity than the much smaller ASA molecule.

Many amino acids are involved in hydrogen binding to ASA and AML. Examples include Lys199 for ASA and Asp255, Asp259 for AML, which are the most important residues in this regard. In the ternary system, (HSA–ASA) AML, AML is able to form a hydrogen bond with Glu311 but ASA does not show any hydrogen binding in the ternary system (HSA–AML)ASA. This suggests that ASA had a lower affinity as a secondary ligand in the mentioned system. The results obtained from molecular modeling indicated that the binding of ASA and AML with HSA were dominated by hydrophobic forces.

HSA contains a single Trp residue at position 214 in subdomain IIA. It was considered as the target to study the effect of the addition of drugs on the synchronous fluorescence spectrum of HSA when $\Delta\lambda=60$ nm [46]. As the efficient energy

transfer from Trp214 to ligands was 2–8 nm, the distance of Trp 214 from the docked ligands was also measured. This was applicable with the high efficient fluorescence quenching of HSA emission in the presence of the second drug. As seen in Table 4, the distance between AML and ASA with Trp214 was about 2.16 and 1.47 nm, respectively, while in the ternary system of (HSA–AML)ASA and (HSA–ASA) AML, the corresponding values were 2.77 and 1.97 (Fig. 11). These data are consistent with the spectroscopic results.

Table 4
Distance of Trp 214 with ASA and AML and also between ASA and AML in binary and ternary systems.

Distance in systems	AML and Trp 214	ASA and Trp 214	AML and ASA
HSA–AML	2.16 nm	–	–
(HSA–ASA)AML	1.97 nm	1.49 nm	2.37 nm
HSA–ASA	–	1.47 nm	–
(HSA–AML)ASA	2.15 nm	2.77 nm	1.45 nm

4. Conclusions

The interactions and competitive binding of ASA and AML to HSA have been studied using different spectroscopic and molecular modeling approaches. The change in the protein conformation upon binding was monitored as a function of the addition of drug by fluorescence, CD and FT-IR spectroscopies. The distance (r) between drugs and the protein was evaluated according to the theory of Forster energy transfer and molecular modeling. Changes in the micro-environment of the aromatic residues were also observed by synchronous fluorescence and three-dimensional spectroscopies. Aggregation of drug/protein complexes was determined through RLS and zeta-potential results. It was clear from the fluorescence and molecular modeling results that the binding of AML and ASA to HSA primarily took place within sub-domain IIA and led to certain changes in the micro-environment of the protein. Results demonstrated that the HSA conformation became altered upon interaction with the first and second drug in the ternary system. The conclusions regarding the effect of one drug on the complex of the other with HSA were presented by comparing the quenching of HSA fluorescence in the binary

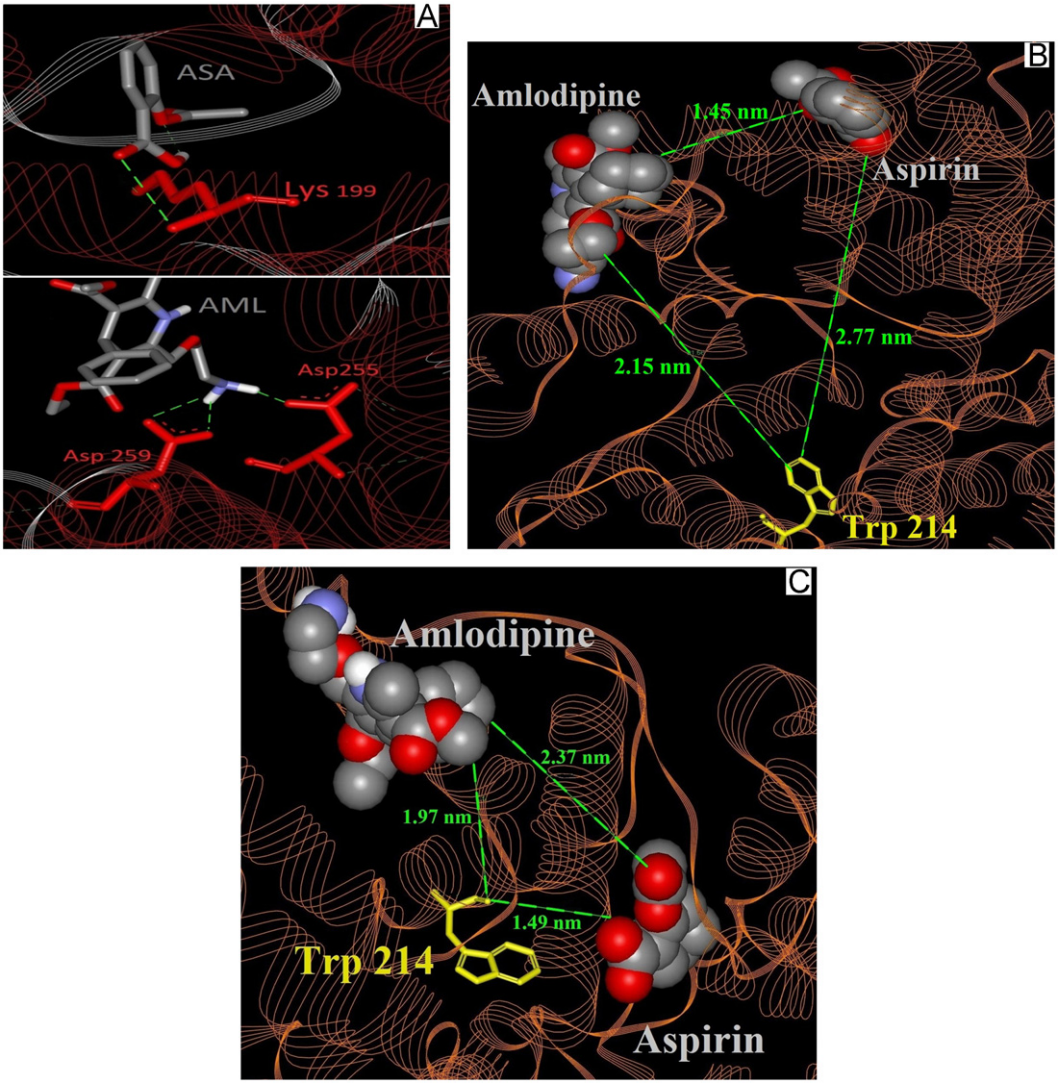

Fig. 11. Computational model of the docking; (A) hydrogen bonds between the residues of HSA with AML and ASA are represented by green dashed lines; (B) distances between the Trp 214 of HSA in (HSA–AML)ASA; (C) (HSA–ASA) AML systems.

and ternary systems and by analyzing the quenching constant values. It was shown that the affinity of HSA to AML was higher than to ASA and that the presence of ASA could cause the decrease of the affinity of AML to HSA in the (HSA–ASA) AML system. On the contrary, in the (HSA–AML)ASA complex, AML and ASA first interacted with each other after which both of the drugs interacted with HSA. In summary, both drugs were able to interact with HSA when administered together but there occurred a mutual influence on their binding with the protein.

Acknowledgments

The financial support of the Research Council of the Mashhad Branch, Islamic Azad University is gratefully acknowledged. The authors thank Dr. Ljungberg for the English editing.

References

[1] P.J. Sinko, Martin's Physical Pharmacy and Pharmaceutical Sciences, Fifth ed., Lippincott Williams & Wilkins, New York, 2006.
[2] M.A. Cheema, P. Taboada, S. Barbosa, J. Juarez, M. Gutierrez-Pichel, M. Siddiq, V. Mosquera, J. Chem. Thermodyn. 41 (2009) 439.
[3] T. Peters Jr, All about Albumin, Academic press, New York, 1996.
[4] K.J. Fehske, W.E. Muller, U. Wollert, J. Biochem. Pharmacol. 30 (1981) 687.
[5] T. Wybranowski, M. Cyrankiewicz, B. Ziomkowska, S. Kruszewski, J. Biosyst. 94 (2008) 258.
[6] R. Artali, G. Bombieri, L. Calabi, A. Del Pra, Farmaco 60 (2005) 485.
[7] F. Yang, C. Bian, L. Zhu, G. Zhao, Z. Huang, M. Huang, J. Struct. Biol. 157 (2007) 348.
[8] H.D. Lewis Jr., J.W. Davis, D.G. Archibald, W.E. Steinke, T.C. Smitherman, J.E. Doherty 3rd, H.W. Schnaper, M.M. LeWinter, E. Linares, J.M. Pouget, S.C. Sabharwal, E. Chesler, H. DeMots, N. Engl. J. Med. 309 (1983) 396.
[9] D.G. Julian, D.A. Chamberlain, S.J. Pocock, J. Br. Med. Assoc. 313 (1996) 1429.
[10] S. Macdonald, Br. Med. J. 325 (2002) 988.
[11] T.D. Warner, J.A. Mitchell, Proc. Natl. Acad. Sci. U. S. A. 99 (2002) 13371.
[12] E.Y. Chew, G.A. Williams, T.C. Burton, F.B. Barton, N.A. Remaley, F.L. Ferris 3rd, Arch. Ophthalmol. 110 (1992) 339.
[13] A.K. Sarkar, D. Ghosh, A. Das, P.S. Selvan, K.V. Gowda, U. Mandal, A. Bose, S. Agarwal, U. Bhaumik, T.K. Pal, J. Chromatogr. B Analyt. Technol. Biomed. Life Sci. 873 (2008) 77.
[14] A.A. Burkin, M.A. Murkin, Prikl. Biokhim. Mikrobiol. 44 (2008) 357.
[15] H.M. Abdel-Wadood, N.A. Mohamed., A.M. Mahmoud, Spectrochim. Acta. A Mol. Biomol. Spectrosc. 70 (2008) 564.
[16] F.C. Bernstein, T.F. Koetzle, G.J. Williams, E.F. Meyer Jr., M.D. Brice, J.R. Rodgers, O. Kennard, T. Shimanouchi, M. Tasumi, J. Mol. Biol. 112 (1977) 535.
[17] S. Sugio, A. Kashima, S. Mochizuki, M. Noda, K. Kobayashi, Protein Eng. 12 (1999) 439.
[18] G.M. Morris, D.S. Goodsell, R.S. Halliday, R. Huey, W.E. Hart, R.K. Belew, A.J. Olson, J. Comput. Chem. 19 (1998) 1639.
[19] HyperChem (TM) Professional 7., Hpercube, Inc., 1115 NW 4th Street, Gainesville, Florida 32601, USA.
[20] S.E. Harding, B.Z. Chowdhry, The Protein–Ligand Interactions: Hydrodynamics and Calorimetry, Oxford University Press, New York, 2001.
[21] C.W. Garland, J.W. Nibler, D.P. Shoemaker, Experiments in Physical Chemistry, 7th ed., McGraw-Hill, Boston, 2003.
[22] A. Sulkowska, B. Bojko, J. Rownicka, W.W. Sulkowski, J. Mol. Struct. 792–793 (2006) 249.
[23] S. Sarzehi, J. Chamani, Int. J. Biol. Macromol. 47 (2010) 558.
[24] J. Chamani, N. Tafrishi, M. Momen-Heravi, J. Lumin. 130 (2010) 1160.
[25] M. Maciazek-Jurczyk, A. Sulkowska, B. Bojko, J. Rownicka, W.W. Sulkowski, J. Mol. Struct. 924–926 (2009) 378.
[26] N.A. Sultan, R.N. Rao, S.K. Nadimpalli, M.J. Swamy, Biochim. Biophys. Acta 1760 (2006) 1001.
[27] P. Daneshgar, A.A. Moosavi-Movahedi, P. Norouzi, M.R. Ganjali, A. Madadkar-Sobhani, A.A. Saboury, Int. J. Biol. Macromol. 45 (2009) 129.
[28] B. Bojko, A. Sulkowska, M. Maciazek-Jurczyk, J. Rownicka, W.W. Sulkowski, Spectrochim. Acta. A Mol. Biomol. Spectrosc. 76 (2010) 6.
[29] B. Bojko, A. Sulkowska, M. Maciazek, J. Rownicka, F. Njau, W.W. Sulkowski, Int. J. Biol. Macromol. 42 (2008) 314.
[30] V. Anbazhagan, R. Renganathan, J. Lumin. 128 (2008) 1454.
[31] J.B.F. Lloyd, J. Nat. 231 (1971) 64.
[32] T. Yuan, A.M. Weljie, H.J. Vogel, J. Biochem. 37 (1998) 3187.
[33] Y.Q. Wang, H.M. Zhang, G.C. Zhang, Q.H. Zhou, Z.H. Fei, Z.T. Liu, Z.X. Li, J. Mol. Struct. 886 (2008) 77.
[34] T. Wang, B.R. Xiang, Y. Li, C.Y. Chen, X.H. Zhou, Z.M. Wang, Y. Dong, Y. Wang, H.S. Fang, J. Mol. Struct. 921 (2009) 188.
[35] E.U. Akusoba, J.N. Miller, J. Proc. Anal. Div. Chem. Soc. 16 (1979) 203.
[36] G. Zhang, Q. Que, J. Pan, J. Guo, J. Mol. Struct. 881 (2008) 132.
[37] H.Q. Chen, F.B. Luo, Y. Liu, A.N. Liang, B. Lin, L. Wang, Spectrochim. Acta. A Mol. Biomol. Spectrosc. 71 (2009) 1701.
[38] H. Yang, Y. Wang, Y. Wang, J. Li, X. Xiao, X. Tan, Spectrochim. Acta A Mol. Biomol. Spectrosc. 71 (2008) 1290.
[39] C.Z. Huang, Y.F. Li, J. Anal. Chim. Acta 500 (2003) 105.
[40] Z. Chen, L. Zhu, T. Song, J. Chen, Z. Guo, Spectrochim. Acta. A Mol. Biomol. Spectrosc. 72 (2009) 518.
[41] Z. Chen, J. Liu, Y. Han, Talanta 71 (2007) 1246.
[42] J. Chamani, J. Mol. Struct. 979 (2010) 227.
[43] X. Long, C. Zhang, J. Cheng, S. Bi, Spectrochim. Acta A Mol. Biomol. Spectrosc. 69 (2008) 71.
[44] C. Yan, J. Tong, D. Xiong, Y. Liu, Z. Pan, J. Anal. Chem. 34 (2006) 796.
[45] J.r. Lakowicz, Principles of Fluorescence Spectroscopy, Third ed., Springer Science +Business Media Inc, New York, 2006.
[46] F. Ding, W. Liu, Y. Li, L. Zhang, Y. Sun, J. Lumin. 130 (2010) 2013.
[47] X. Hu, S. Cui, J. Liu, Spectrochim. Acta A Mol. Biomol. Spectrosc. 77 (2010) 548.
[48] A.P. De-Silva, H.Q. Gunaratne, T. Gunnlaugsson, A.J. Huxley, C.P. McCoy, J.T. Rademacher, T.E. Rice, Chem. Rev. 97 (1997) 1515.
[49] I. Vaya, R. Perez-Ruiz, V. Lhiaubet-Vallet, M.C. Jimenez, M.A. Miranda, Chem. Phys. Lett. 486 (2010) 147.
[50] F.L. Cui, J. Fan, W. Li, Y.C. Fan, Z.D. Hu, J. Pharm. Biomed. Anal. 34 (2004) 189.
[51] Y. Liu, X. Jiang, Z. Yang, X. Zheng, J. Liu, T. Zhou, Appl. Spectrosc. 64 (2010) 980.
[52] F.Y. Wu, L.N. Zhang, Z.J. Ji, X.F. Wan, J. Lumin. 130 (2010) 1280.
[53] B. Valeur, J.C. Brochon, New Trends in Fluorescence Spectroscopy, Springer press, Berlin, 1999.
[54] B. Valeur, Molecular Fluorescence: Principles and Applications, Wiley press, New York, 2001.
[55] G.D. Fasman, Circular Dichroism and the Conformational Analysis of Biomolecules, Plenum Press, New York, 1996.
[56] D. Whitford, The Proteins Structure and Function, John Wiley &Sons, West Sussex, 2005.
[57] I. Matei, M. Hillebrand, J. Pharm. Biomed. Anal. 51 (2010) 768.
[58] P. Yang, F. Gao, The Principle of Bioinorganic Chemistry, Science Press, Beijing, 2002.
[59] D. Li, J. Zhu, J. Jin, X. Yao, J. Mol. Struct. 846 (2007) 34.
[60] Y. Li, W. He, Y. Dong, F. Sheng, Z. Hu, J. Bioorg. Med. Chem. 14 (2006) 1431.
[61] Y. Li, W. He, H. Liu, X. Yao, Z. Hu, J. Mol. Struct. 831 (2007) 144.
[62] P.N. Naik, S.A. Chimatadar, S.T. Nandibewoor, J. Photochem. Photobiol. B. 100 (2010) 147.
[63] T.K. Maiti, K.S. Ghosh, J. Debnath, S. Dasgupta, Int. J. Biol. Macromol. 38 (2006) 197.
[64] H Gao, L Lei, J Liu, Q Kong, X Chen, Z Hu, J. Photochm. Photobiol. A Chem. 167 (2004) 213.
[65] R. Xu, J. Particuol. 6 (2008) 112.
[66] S. Roessler, R. Zimmermann, D. Scharnweber, C. Werner, H. Worch, Colloids Surf. B Biointerfaces 26 (2002) 387.
[67] M. Mirnezami, L. Restrepo, J.A. Finch, J. Colloid Interface Sci. 259 (2003) 36.
[68] K. Cai, M. Frant, J. Bossert, G. Hildebrand, K. Liefeith, K.D. Jandt, Colloids Surf. B Biointerfaces 50 (2006) 1.
[69] G. Prieto, J. Sabin, J.M. Ruso, A. Gonzalez-Perez, F. Sarmiento, Colloids Surf. A Physicochem. Eng. Aspects 249 (2004) 51.
[70] C. Weber, C. Coester, J. Kreuter, K. Langer, Int. J. Pharm. 194 (2000) 91.
[71] M.A. Cheema, P. Taboada, S. Barbosa, M Gutierrez-Pichel, E. Castro, M. Siddiq, V. Mosquera, J. Colloids Surf. B Biointerfaces 63 (2008) 217.
[72] L. Trynda-Lemiesz, M. Luczkowski, J. Inorg. Biochem. 98 (2004) 1851.
[73] Z. Bikadi, E. Hazai, F. Zsila, S.F. Lockwood, J. Bioorg. Med. Chem. 14 (2006) 5451.
[74] X.M. He, D.C. Carter, Nature 358 (1992) 209.